

# Electrochemical Behaviour of Aluminum - Fly Ash Composites Produced by Powder Metallurgy Technique

**E. Marin<sup>1</sup>, M. Lekka<sup>1</sup>, F. Andreatta<sup>1</sup>, L. Fedrizzi<sup>1</sup>, A. Moutsatsou<sup>2</sup>, G. Itskos<sup>2</sup>, N. Kouloumbi<sup>2</sup>**

<sup>1</sup> University of Udine, Department of Chemical Science and Technologies, Via del Cotonificio 108, 33100, Udine, Italy

<sup>2</sup>National Technical University of Athens, School of Chemical Engineering, 9 Heroon Polytechniou Street, Zografou Campus, 15773, Athens, Greece

**KEYWORDS:** calcareous fly ash, aluminum, Metal Matrix Composites (MMCs), electrochemical behaviour

## ABSTRACT

In this study, an ASTM Class C 618 highly calcareous fly ash (FA) was used for the production of Metal Matrix Composites (MMCs) using Powder Metallurgy (PM) technique. Aluminum-FA composites containing 10 and 20 wt. % FA were prepared and compacted. The green products were then sintered for 2 h at 600 °C. Sintered Al-FA MMCs showed an increase in hardness and wear suggesting their possible use in industrial applications for example in covers, casings, brake rotors or engine blocks. Most possible applications of MMCs not only require wear resistance, but also corrosion resistance in different mild aggressive medias. For this reason, a complete electrochemical characterization of FA MMCs was performed. Polarization Curves in NaCl solution were performed on polished Aluminum and Aluminum-FA samples in order to evaluate and compare their resistance to localized corrosion. To explain the clear differences between samples, morphological and Volta Potential maps were acquired using Scanning Kelvin Probe Force Microscopy (SKP-FM). Using SKP-FM, particles and phases with different Surface Potential respect to the metal matrix were identified. On the same surface areas, Scanning Electron Microscopy (SEM) maps were acquired and Energy Dispersive X-ray Spectroscopy (EDXS) analyses were performed to determine the quantitative composition of the different phases. The same specimens have been immersed in a NaCl solution. At different time intervals the samples have been extracted from the corrosive media and both SKP-FM and EDXS measurements have been repeated on their surface to evaluate the consequences of immersion.

## INTRODUCTION

Metal matrix composites (MMCs) based on aluminum alloys can be considered for structural applications providing improved physical, mechanical and tribological properties relative to unreinforced aluminum alloys. In particular, MMCs reinforced with ceramic fibers or particles can offer improved strength, stiffness, hardness and damping

capacity<sup>1-5</sup>. Among the various discontinuous reinforcement used, fly ashes (FAs) have been recently considered for the production of MMCs<sup>6-9</sup>. FAs can be employed as inexpensive strengthening particles for the aluminum matrix increasing wear resistance<sup>10,11</sup>. Moreover, FAs present low density. MMCs based on aluminum alloys reinforced with FAs can be produced by powder metallurgy, liquid metal stir casting and infiltration techniques<sup>12,13</sup>. Al-based MMCs reinforced with FA have potential applications as covers, pans, casings, pulleys, manifolds, valve covers, brake rotors and engine blocks in automotive, small engine and electromechanical industry sectors<sup>10-11,14</sup>.

A critical aspect related to engineering application of aluminum-based MMCs is the influence of the reinforcement on the overall corrosion resistance of the composite material<sup>15-19</sup>. This is related to the strongly heterogeneous microstructure of MMCs, which can lead to localized attack, mainly in the form of pitting or crevice corrosion. This attack might be related to galvanic coupling between second phases and the aluminum matrix. Localized corrosion attack in the region surrounding cathodic intermetallics is well known for aluminum alloys<sup>20</sup>. The electrochemical behaviour of commercially pure aluminum is significantly affected by the existence of Fe-rich intermetallics (constituent particles), which may act as initiation sites for localized corrosion in aggressive solutions containing chlorides<sup>21</sup>. Fe-rich intermetallics behave as cathodes and establish a local high pH in the surrounding region<sup>22</sup>. This leads to fast dissolution of the aluminum matrix resulting in pitting corrosion. Moreover, it is possible that there is an interaction between clusters of intermetallics creating conditions that further promote localized attack.

Aluminum matrix composites might be subjected also to localized corrosion. Porosity and voids at the interface between reinforcement and aluminum matrix are reported to be preferential sites for localized corrosion in MMCs reinforced with ceramic fibers or particles<sup>15</sup>. In particular, pitting susceptibility of MMC based on aluminum alloy AA1050 reinforced with silicon carbide particles is strongly associated to crevices at the matrix/reinforcement interface<sup>15</sup>. Crevices can arise from poor interface bonding or by cracks in the reinforcement. Moreover, the propagation of pitting attack might be influenced by the reinforcement geometry. The interface region between the reinforcement and the matrix might be possibly affected by the active behaviour of the interface region resulting from reactions occurring during material processing<sup>15</sup>. This is a critical aspect for the production of MMCs reinforced with FAs, which might contain different reactive species that can locally modify the electrolyte (pH, concentration of aggressive species) in aggressive solutions<sup>13</sup>.

This paper aims to study the effect of high calcareous Class C FAs on the electrochemical behaviour of MMCs based on aluminum matrix produced by powder metallurgy. In particular, it focuses on the effect of different phases detected in FA-Al-MMCs relating localized corrosion susceptibility to the complex microstructure of the material.

## EXPERIMENTAL

Commercially pure Aluminum powder (99.80 wt. %, 325mesh, chemical composition presented in Table 1) was selected as the metal matrix of the composites. The fly ashes

that were used as reinforcement materials were collected from the electrostatic precipitators of the lignite-fired power stations of Kardia, Northern Greece. Kardia Fly-Ash (KFA) is a high calcareous, Class C ash according to ASTM C 618. The chemical composition of KFA is presented in Table 2. Al-fly ash mixtures, containing 10 and 20 wt. % ground KFA particles (<56  $\mu\text{m}$ ) were prepared and compacted using cold axial pressing (applied pressure: 7 tons). The preparation stage included ultrasonic vibration and mechanical blending in order to achieve a high homogeneity level. The composites were sintered at 600°C for 2h in an inert atmosphere under constant flow of nitrogen. The sintering process parameters have been chosen based on the previously reported results<sup>13</sup>.

| Table 1: Chemical composition of the Al powder |       |
|--|-------|
| Element  | %     |
| Al   | 99.80 |
| Fe   | 0.091 |
| Si   | 0.025 |
| Cu   | 0.001 |
| Mn   | 0.003 |
| Pb   | 0.001 |
| Mg   | 0.001 |
| Zn   | 0.009 |
| Ni   | 0.004 |
| Ti   | 0.004 |
| Zr   | 0.051 |
| Cr   | 0.001 |
| Ga   | 0.007 |

| Table 2: Chemical composition of KFA |       |
|--------------------------------------|-------|
| Compound                             | %     |
| SiO <sub>2</sub>                     | 30.16 |
| Al <sub>2</sub> O <sub>3</sub>       | 14.93 |
| Fe <sub>2</sub> O <sub>3</sub>       | 5.10  |
| CaO                                  | 34.49 |
| Na <sub>2</sub> O                    | 1.01  |
| K <sub>2</sub> O                     | 0.40  |
| MgO                                  | 2.69  |
| P <sub>2</sub> O <sub>5</sub>        | 0.34  |
| TiO <sub>2</sub>                     | 0.60  |
| SO <sub>3</sub>                      | 6.28  |
| MnO                                  | 0.07  |
| LOI                                  | 3.95  |

The sintered samples were grinded using abrasive SiC paper under a constant liquid ethanol jet in order to prevent a possible dissolution of the Fly Ash phases or corrosion phenomena caused by the contact with water. Polishing was then performed using diamond suspensions in order to obtain a final surface roughness of about 20 nm Ra. After polishing, the samples were cleaned in an ethanol ultrasonic bath for about 15 minutes and then heat-dried in a heat sterilizer at constant temperature of 50°C.

A Veeco Multimode Nanoscope IIIa Atomic Force Microscope (AFM) was used to map the samples surface. Morphological and Surface Volta Potential maps were simultaneously obtained using a Scanning Kelvin Probe Force Microscopy (SKP-FM) configuration on marked 100x100 µm areas. SKP-FM gives information about the anodic and/or cathodic behaviour of the different particles and phases present on the sample's surface. On the same areas, observations were then performed using a Karl Zeiss EVO-40 Scanning Electron Microscope (SEM) in backscattered electrons configuration (BSE), which provides a clear overview of the particle dimensions and distribution inside the metal matrix. Energy Dispersive X-Ray Spectroscopy (EDXS) was used in order to obtain a semi-quantitative compositional analysis of the different phases present on the sample surface.

The corrosion resistance of the different samples was firstly evaluated by potentiodynamic polarization curves in a 0.05 M NaCl solution. Measurements were performed under a three electrode configuration according to the ASTM G3-89, with Ag/AgCl as Reference Electrode (RE) and a platinum wire as a Counter Electrode (CE). The equipment used was an Autolab PGSTAT-20 potentiostat. A 0.2 mV/s scan rate was employed. Open Circuit Potential (OCP) was measured for 15 minutes before starting the test and then the potential has been scanned starting from -0.2 V vs. OCP. The measurement was stopped when a corrosion current density of about 0.01 A/cm<sup>2</sup> was reached, considered indicative for a fast corrosion degradation of the sample surface. Three potentiodynamic polarization curves were recorded for each sample.

Immersion tests were carried out in a 0.05 M NaCl solution for 200h using a vertical configuration electrochemical cell and a 10mm diameter o-ring to prevent solution leakage. Vertical sample positioning was considered fundamental in order to avoid re-deposition of corrosion products on the surface, which may act as an insulator for the underneath metallic surface. Samples were extracted from the electrolyte every 50h in order to be analyzed by SEM-EDXS. The morphological and compositional modifications induced by the prolonged contact with the sodium chloride containing solution were monitored to discriminate the different corrosion phenomena.

## RESULTS AND DISCUSSION

Fig. 1 shows an AFM topographic map, a SKPFM Volta potential map and SEM-BSE micrograph for the same representative area of sintered Al sample.

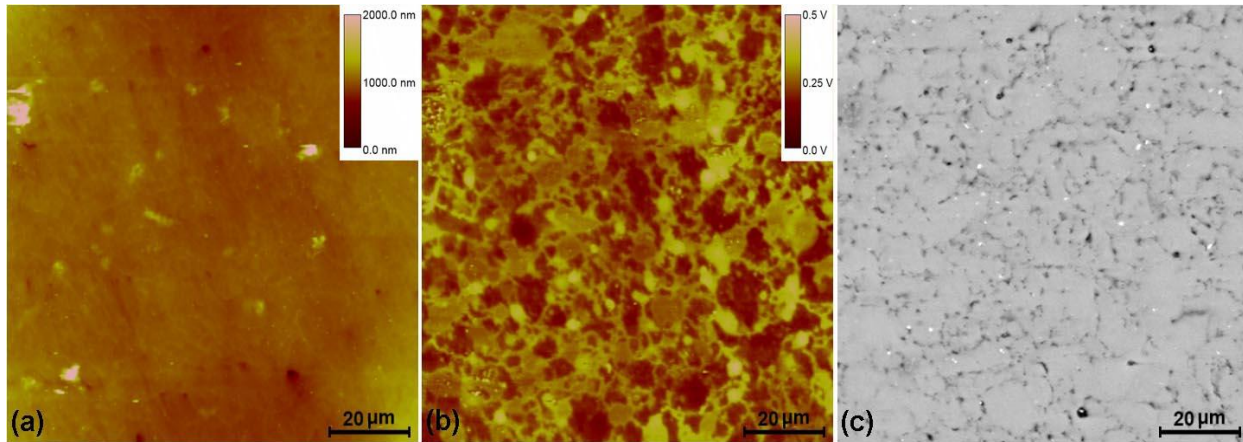


**Fig. 1: (a) AFM topographic map, (b) SKPFM Volta potential map and (c) SEM-BSE micrograph of the sintered Al sample**

The topographic map (Fig. 1a) of the sintered Al sample evidences the typical morphology for a polished sample. Some features higher than the matrix (bright spots) as well as lower than the matrix (dark spots) could be recognized. Bright spots can be associated with the presence of particles on the sample surface, while dark spots can be associated with the residual porosities left by the sintering process. The Volta potential map (Fig. 1b) reveals the grain structure of the material. Regions with different Volta potential could be clearly identified, most likely corresponding to different grains. Moreover, the grain boundaries exhibit higher potential (brighter) than the grain interior. This behaviour might be related to the oxidation of the Al powder during the production process.

The SEM micrograph (Fig. 1c) exhibits the same grain structure observed in the Volta potential map. Moreover, the SEM micrograph reveals the existence of small intermetallic particles (small bright and dark phases) with size of few micrometers. These intermetallics are most likely Fe-rich phases ( $\text{Al}_3\text{Fe}$  or  $\text{Al}_6\text{Fe}$ ). The existence of intermetallic phases (constituent particles) in aluminum alloys is well known in literature and is related to the chemical composition of the material<sup>21,22</sup>. The same intermetallic particles visible in the SEM micrograph can be identified in the Volta potential map. As can be seen in the Volta Potential map (Fig. 1b), the intermetallics often exhibit higher potential than the surrounding matrix. This indicates that the intermetallics display cathodic behaviour relative to the matrix and thus might promote a localized corrosion attack of the surrounding region due to the formation of localized galvanic couples.

Fig. 2 shows an AFM topographic map, a SKPFM Volta potential map and SEM-BSE micrograph for the same representative area of the Al + 10% KFA sample.

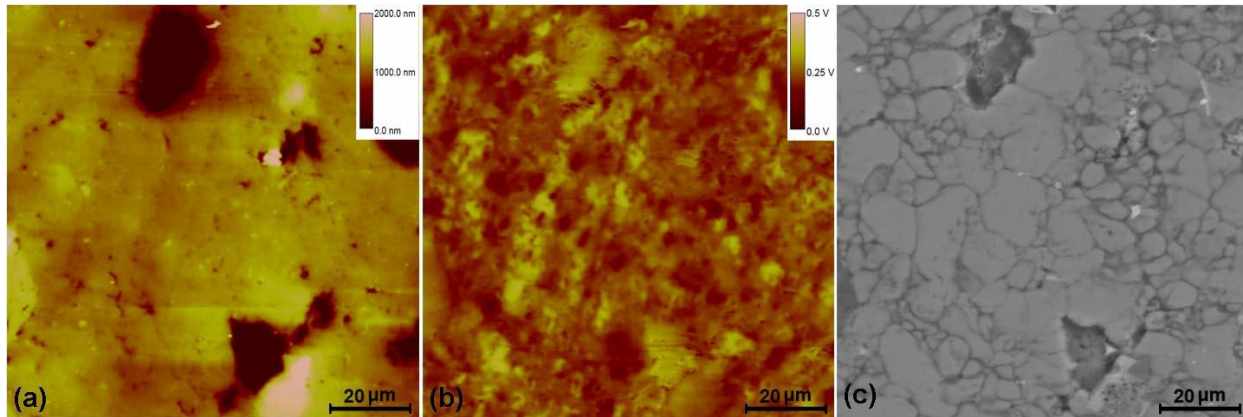


**Fig. 2: (a) AFM topographic map, (b) SKPFM Volta potential map and (c) SEM-BSE micrograph of the Al + 10% KFA sample**

The topographic map (Fig. 2a) of the sintered Al 10% KFA sample shows dark regions, lower than the surrounding material which, according to the SEM micrograph (Fig. 2c) can be associated to FA phases. The Volta potential maps (Fig. 2b) indicate that these FA phases present a higher potential than the matrix. Moreover, the metal matrix grain boundaries exhibit higher potential than their interior as already observed for the pure Al samples.

The composite sample microstructure is much more evident in the SEM micrograph (Fig. 2c). In addition to the large FA particles there are smaller ones randomly distributed into the metal matrix and preferentially located at the Al grain boundary regions. Moreover, relatively small Fe-rich intermetallics can be identified in the SEM micrograph (Fig. 2c) as already observed in pure Al samples (Fig. 1c).

Fig. 3 shows an AFM topographic map, a SKPFM Volta potential map and SEM-BSE micrograph for the same representative area of the Al + 20% KFA sample.

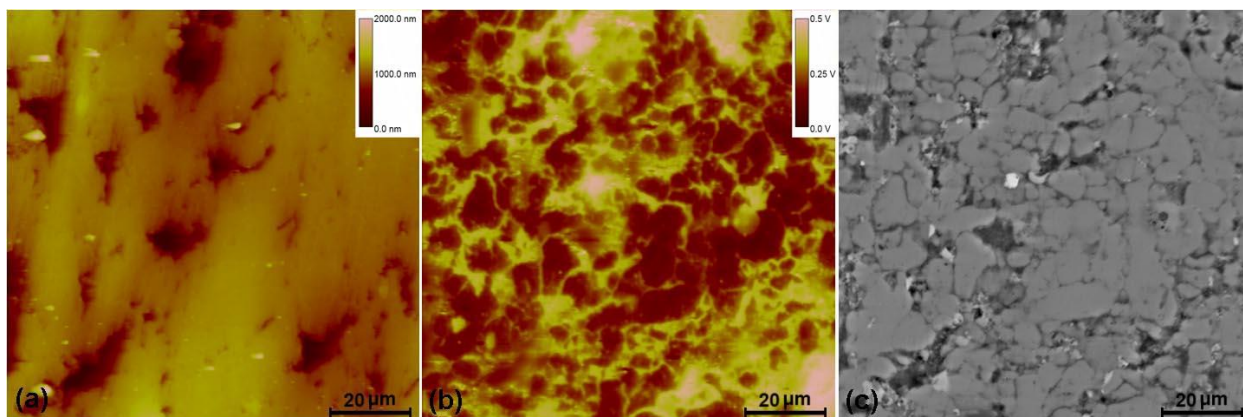


**Fig. 3: (a) AFM topographic map, (b) SKPFM Volta potential map and (c) SEM-BSE micrograph of the Al + 20% KFA sample**

The topographic map (Fig. 3a) of the sintered Al 20% KFA sample shows dark spots that can be associated to large FA particles. The few big FA particles which appear

lower than the metal matrix on the topographic map exhibit higher potential relatively to the surrounding Aluminum matrix.

The grain boundaries also display higher potential than the grain interior in line with the results obtained for the pure Al sample. However the potential difference between the grain boundaries and the interior appears higher for this sample compared to the previously analyzed ones. This behavior might be related to segregation or precipitation at the grain boundaries of second phases due to the high fraction of FA.

The Volta potential map (Fig. 3b) is consistent with the SEM micrograph (Fig. 3c). The sample displays randomly distributed large FA particles, smaller FA particles preferentially located at the metal matrix grain boundaries and small Fe-rich intermetallics.

Potentiodynamic polarization curves were well reproducible for all samples. Representative potentiodynamic polarization curves for pure Al, Al10%KFA and Al20%KFA samples are reported in Fig. 4.

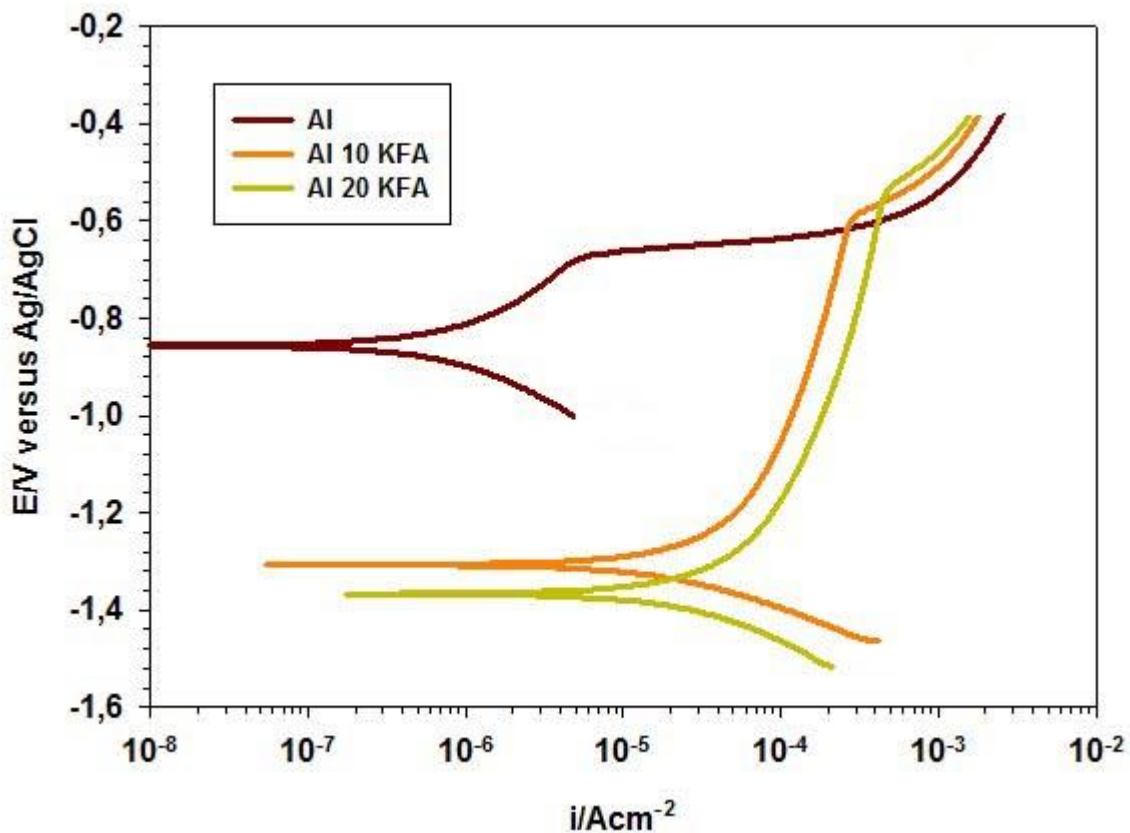


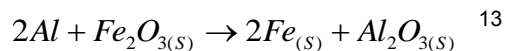
Fig. 4: Representative potentiodynamic polarization curves of the three different specimen

The potentiodynamic polarization curve relative to the pure Al sample (Fig. 4) exhibits a corrosion potential of about -0.86 V vs Ag/AgCl. The corrosion current density is about  $10^{-6}$  A/cm<sup>2</sup>. The curve displays a passive behaviour with breakdown potential at -0.650

V vs. Ag/AgCl. The potentiodynamic polarization curves relative to the aluminum matrix composite samples (Al 10% KFA and Al 20% KFA) exhibit a corrosion potential of about -1.3 V vs Ag/AgCl and a corrosion current density of about  $2 \cdot 10^{-5}$  A/cm<sup>2</sup> for both samples. Moreover, the trend of the current density is very similar for the two aluminum matrix composite samples. The composite samples do not show a passive behaviour in the potentiodynamic polarization scan and exhibit a sharp increase of the current density at potential values close to the pitting potential of the pure Al samples.

The corrosion potential of the Al 10%KFA and Al 20%KFA samples (Fig. 4) is more negative than that of the pure aluminum sample. Moreover, the Al 10%KFA and Al 20%KFA samples exhibit higher (about one order of magnitude) corrosion current density than the pure Al sample. In particular, the composite samples do not show passive behaviour in potentiodynamic polarization tests. This is an indication that the introduction of FA particles lead to an overall decrease of the corrosion resistance of the system relative to the pure aluminum sample. In particular, the shift of the corrosion potential in the direction of negative potentials and the increase of the corrosion current density is related to the introduction of FA in the aluminum matrix. The current density increase visible at about -0.6 V vs Ag/AgCl might be related to localized attack of the aluminum matrix, as observed for the potentiodynamic polarization curve relative to the pure Al sample.

The corrosion behaviour of the MMCs might be mainly correlated to two different phenomena: the possible parallel oxidation reactions of sintered FA phases such as Fe and FeO to Fe<sub>2</sub>O<sub>3</sub> and/or Fe<sub>3</sub>O<sub>4</sub>. It is indeed known that Fe is present in the FA as Fe<sub>2</sub>O<sub>3</sub>, but during sintering it may react with Aluminum according to:



Following this reaction, after sintering Fe can be present into the sintered samples as metallic Fe or as FeO due to air oxidation. Furthermore, the high corrosion current density of the composite samples might be related to activation phenomena due to a localized pH variation at the FA/metal interface. It is in fact known that the KFA has a pH between 11.2 and 11.7, interval in which the Al does not exhibit passive behaviour. For this reason, local pH variations might impair the passivity of the Al metal matrix leading to severe Al dissolution.

SEM micrographs of a sintered Al representative area are reported in Fig. 5 before and after different immersion times in the corrosive media.

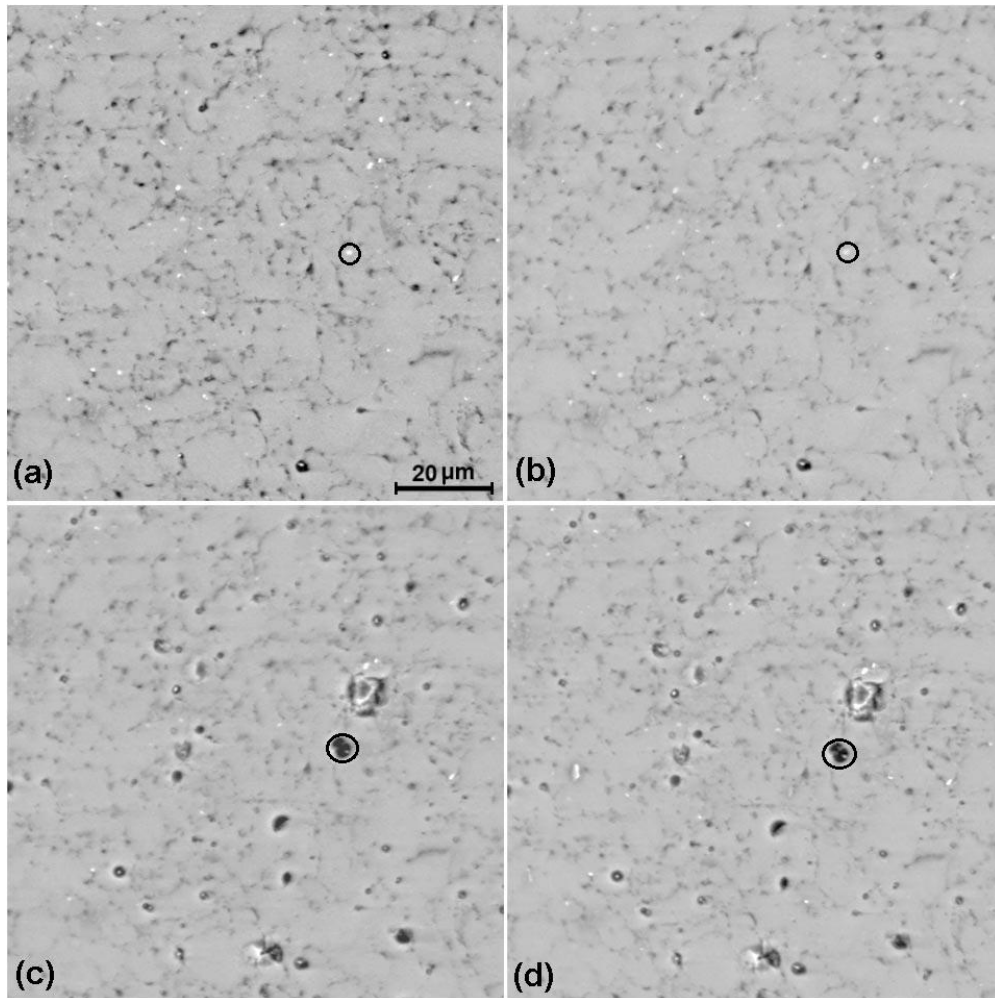


**Fig. 5: SEM micrographs of a pure Al sample representative surface area (a) before the immersion in the electrolyte and after (b) 50h, (c) 100h, (d) 200h of immersion.**

The SEM micrographs acquired before the immersion (Fig. 5a) and after 50h of immersion (Fig. 5b) show a similar morphology. In particular no evident signs of corrosion can be individuated in Fig. 5b. After longer times of immersion (Fig. 5c, 5d) localized corrosion attacks become visible at locations near the second phase particles. EDXS spectra have been acquired on the particles showing that these are most likely Fe-rich intermetallics. Representative analyses results acquired on the marked area of Fig. 5 are reported in Table 3.

| Table 3: EDXS localized analyses results on the marked area of Fig. 5 (wt.%) |       |       |      |      |      |
|--|-------|-------|------|------|------|
| Immersion time (h)   | O     | Al    | Cl   | Ni   | Fe   |
| 0  | 4.39  | 88.74 |      | 0.32 | 5.04 |
| 50   | 4.90  | 87.37 |      | 0.26 | 4.68 |
| 100  | 18.27 | 80.21 | 0.44 |      | 0.26 |
| 200  | 17.73 | 79.70 | 0.20 |      |      |

As can be observed from the SEM micrographs and the relative EDXS analyses, localized corrosion mainly occurs at the location of cathodic intermetallics due to the galvanic coupling with the aluminum matrix. This causes localized dissolution of the Al matrix in the region surrounding the intermetallic particles. After longer immersion times, the localized corrosion at the intermetallic sites might cause the detachment of the particles thus leading to the formation of pits on the sample surface. Indeed the pit formation is evident in Fig. 5c and 5d and the relative EDXS analyses revealed the decrease and final disappearance of the Fe signal confirming the detachment of the Fe-rich intermetallic particle.

SEM micrographs of a Al with 10% of KFA specimen representative area are reported in Fig.6 before and after different immersion times in the corrosive media.

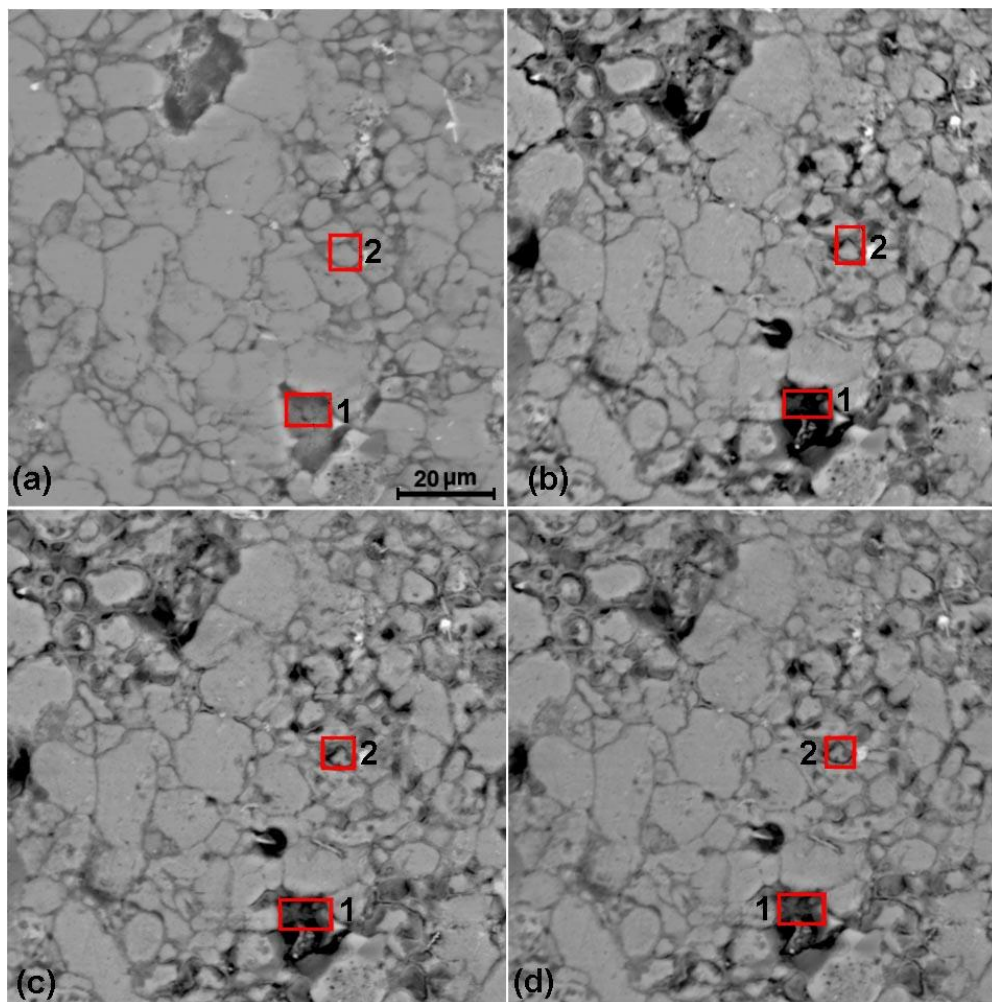


**Fig. 6: SEM micrographs of a Al/10% KFA sample representative surface area (a) before the immersion in the electrolyte and after (b) 50h, (c) 100h, (d) 200h of immersion**

From the SEM micrographs it is evident that the immersion in the NaCl electrolyte causes a localized corrosion which interests mainly the areas surrounding the FA phases and it is more intense with respect to the pure aluminum sample. This is clearly visible comparing Fig. 6a and Fig. 6b. A number of dark spots appear onto the surface,

mainly in proximity of partially exposed FA particles. The Fe-rich intermetallics are most likely still present in the metal matrix (small white spots) and a localized corrosion attack at the interface metal matrix – intermetallics is still evident but less severe than that occurring near the FA particles. In addition the large FA particles are most likely undergone partial dissolution which becomes more evident for longer immersion times (Fig. 6c, 6d) In order to better understand the degradation mechanisms, EDXS analyses have been performed on different zones of the sample area. The results of the analyses acquired on the marked area 1 of Fig. 6 for different immersion times are reported in Table 4.

| Immersion time (h) | O     | Mg   | Al    | Si   | S    | K    | Ca    | Ti   | Fe   |
|--------------------|-------|------|-------|------|------|------|-------|------|------|
| 0                  | 52.24 | 0.35 | 3.66  | 0.53 | 1.77 | 0.25 | 40.86 |      | 0.33 |
| 50                 | 29.26 | 1.32 | 43.90 | 5.75 |      | 0.27 | 13.48 | 0.34 | 4.42 |
| 100                | 31.36 | 1.57 | 36.32 | 7.67 |      | 0.29 | 16.12 | 0.26 | 5.55 |
| 200                | 37.74 | 1.22 | 34.24 | 9.41 |      | 0.34 | 12.26 | 0.32 | 3.95 |

The EDXS analysis performed before the immersion in the electrolyte reveals the presence of a high amount of Ca which might be present either as  $\text{CaSiO}_3$  or as  $\text{CaO}$ <sup>13</sup>. However, low amounts of S, Si, Fe and Mg can be detected in this area as well. This corresponds to the typical composition of FAs.

After 50h of immersion there is a complete dissolution or detachment of S containing phases and a noticeable decrease of the Ca signal. This might be attributed to the dissolution of the  $\text{CaSiO}_3$  phase, which is soluble in NaCl solutions. As a consequence there is an increase of the Al, Si and Fe signals. The SEM micrographs (Fig. 6b-d) show also an intense dissolution of the aluminum matrix around the analyzed area, which might be related to a local increase of the solution pH.

The results of the EDXS analyses acquired on the marked area 2 of Fig. 6 are reported on Table 5.

| Immersion time (h) | O     | Mg   | Al    | Si   | S    | K    | Ca    | Fe   |
|--------------------|-------|------|-------|------|------|------|-------|------|
| 0                  | 19.41 |      | 62.22 | 0.87 | 1.79 | 0.21 | 13.15 | 1.46 |
| 50                 | 37.11 | 1.05 | 37.14 | 9.35 |      | 0.24 | 11.94 | 2.26 |
| 100                | 36.35 | 0.70 | 45.64 | 6.80 |      | 0.26 | 7.75  | 1.80 |
| 200                | 35.65 |      | 59.47 | 0.50 |      | 0.29 | 0.21  | 0.97 |

Before the immersion in the electrolyte Al grains are observed on the marked area 2 (Fig. 6a). The EDXS analysis acquired on these grains shows a high amount of Al together with a relevant amount of Ca as well as low amounts of Si, S and Fe. This leads to the hypothesis that FA particles are located immediately below the visible Al grains. After the first 50h of immersion, these particles became visible due to the

dissolution of the Al matrix. Indeed the EDXS analyses reveal an increase of all elements present in the FA except from S and Ca. Also in this case the S containing phases are completely dissolved after 50h of immersion, while the slight decrease of the Ca signal might be attributed to a partial dissolution of the  $\text{CaSiO}_3$  phase. After longer times of immersion the Al matrix is subjected to dissolution due to crevice corrosion leading to the detachment of the FA particles.

The degradation morphology observed by SEM and the relative EDXS analyses after different times of immersion suggest the following degradation mechanisms: 1) The FA particles undergo a partial dissolution of the phases soluble in the NaCl electrolyte. 2) The aluminum matrix surrounding the FA particles is subjected to crevice corrosion. 3) Galvanic coupling between the Fe-rich intermetallics and the matrix leads to localized Al dissolution. Based on the morphology shown in Fig. 6 it might be stated that the dissolution of the soluble FA phases and the crevice corrosion are the main degradation mechanisms.

SEM micrographs of a Al with 20% of KFA specimen representative area are reported in Fig.6 before and after different immersion times in the corrosive media.

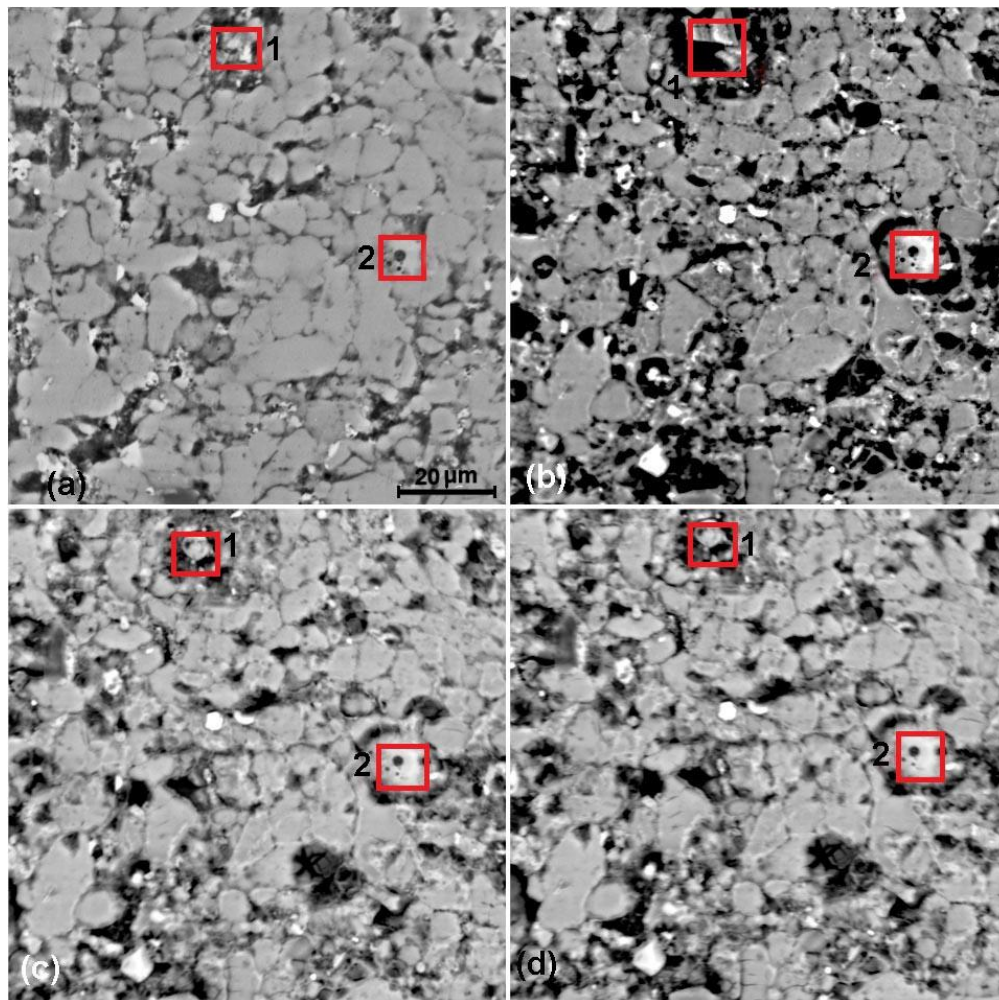


**Fig. 7: SEM micrographs of a Al/20%KFA sample representative surface area (a) before the immersion in the electrolyte and after (b) 50h, (c) 100h and (d) 200h of immersion.**

The SEM micrograph of Fig. 7b shows that the composite specimen exhibits strong localized attack after only 50h of immersion. It is evident that the higher amount of FA particles in the metal matrix might cause a more intense degradation after the immersion in the electrolyte in comparison to the Al/10%KFA samples (Fig. 6b). There is, also in this case, a partial dissolution of the large FA particles and a Al matrix dissolution at the areas surrounding the FA particles. EDXS analyses have been performed on different zones of the sample surface. The results of the analyses acquired in the marked area 1 of Fig. 7 are reported in Table 6.

| Immersion time (h) | O     | Mg   | Al    | Si   | S    | K    | Cl   | Ca    | Fe   |
|--------------------|-------|------|-------|------|------|------|------|-------|------|
| 0                  | 30.88 |      | 49.35 | 1.03 | 2.36 |      |      | 14.84 | 0.90 |
| 50                 | 59.51 |      | 12.05 | 0.80 |      |      | 0.64 | 26.37 | 0.63 |
| 100                | 40.18 | 0.76 | 51.75 | 2.93 |      | 0.18 | 0.29 | 1.67  | 1.65 |
| 200                | 41.48 | 0.75 | 49.65 | 3.23 |      | 0.20 | 0.29 | 1.99  | 1.81 |

Before the immersion the EDXS analysis reveals a high amount of Al and Ca related to a Ca rich FA particle embedded in the Al matrix. After only 50h of immersion there is a significant decrease of the Al content and a significant increase of the Ca content. The morphological observation (Fig. 7b) reveals the formation of crystals in the region of the large pore, which is probably formed due to the dissolution of the surrounding material. Moreover, the S containing phases are completely dissolved or detached also in this case. After longer immersion times, the Ca signal presents a drastic decrease that might be attributed to the dissolution of the  $\text{CaSiO}_3$  phase. The crystals visible in Fig. 7b can not be distinguished in Fig. 7c and 7d. SEM micrographs of the same area at higher magnification are reported in Fig. 8.

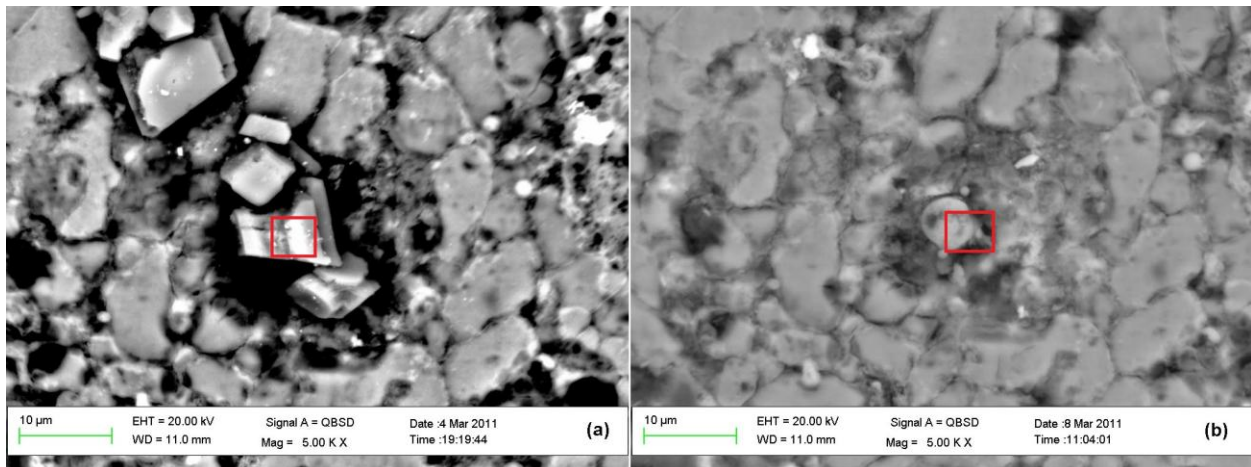


Fig. 8: SEM micrographs the Fig. 7 zone 1 surface area after (a) 50h and (b) 100h of immersion in the electrolyte

As can be observed in Fig. 8, there is the formation of crystals in the center of the hole after 50h of immersion, which has been probably created due to the dissolution of the

surrounding metal matrix. After 100h of immersion these crystals have been detached and extensive precipitation of corrosion products probably occurs in the hole. The EDXS analyses results on the marked area of Fig. 8 are reported in Table 7.

| Immersion time (h) | O     | Mg   | Al    | Si    | K    | Ca   | Ti   | Fe   |
|--------------------|-------|------|-------|-------|------|------|------|------|
| 0                  | 20.31 |      | 70.54 | 1.11  | 0.32 | 5.31 | 0.11 | 2.30 |
| 50                 | 51.32 | 1.57 | 18.78 | 14.75 | 1.46 | 8.20 | 0.27 | 3.65 |
| 100                | 49.83 | 1.48 | 21.79 | 13.96 | 1.51 | 7.10 | 0.26 | 4.07 |
| 200                | 49.08 | 1.60 | 21.16 | 14.92 | 1.48 | 7.45 | 0.33 | 4.00 |

It is evident that the formed crystals are composed by a Ca rich phase, probably  $\text{CaCl}_2$  due to the dissolution of the  $\text{CaSiO}_3$  phase. After 100h of exposure the Ca amount is really low. This leads to the hypothesis that the crystals have been detached and the hole has been filled in by Al and Si hydroxides formed due to the dissolution of both  $\text{CaSiO}_3$  and surrounding metal.

The EDXS analyses results on the area 2 of Fig. 7 are reported in Table 6.

| Immersion time (h) | O     | Mg   | Al    | Si   | K    | Cl   | Ca    | Fe   |
|--------------------|-------|------|-------|------|------|------|-------|------|
| 50                 | 65.99 |      | 2.40  | 0.34 |      | 0.68 | 30.59 |      |
| 100                | 51.86 | 1.12 | 36.02 | 6.66 | 0.44 | 0.13 | 2.13  | 1.64 |

This area contains a spherical particle which is firmly embedded into the metal matrix before the immersion. Indeed the EDXS analysis before the immersion reveals a high amount of Al and small amounts of Si, Ca, Ti and Fe suggesting the existence of a FA particle. After 50h of immersion (Fig. 7b) dissolution of the aluminum surrounding the particle is noticed. The Al matrix dissolution becomes more evident after longer times of immersion while the FA particle remains unaffected as demonstrated by the EDXS analyses. Based on the morphology and the chemical composition of the FA particle, it might be deduced that it is a Si rich stable FA particle that has not reacted with the metal matrix during sintering as it is covered by an amorphous glass layer of  $\text{SiO}_2$ <sup>23</sup>. This could lead to a preferential dissolution of the Al matrix at the interface due to crevice corrosion (Fig. 9).

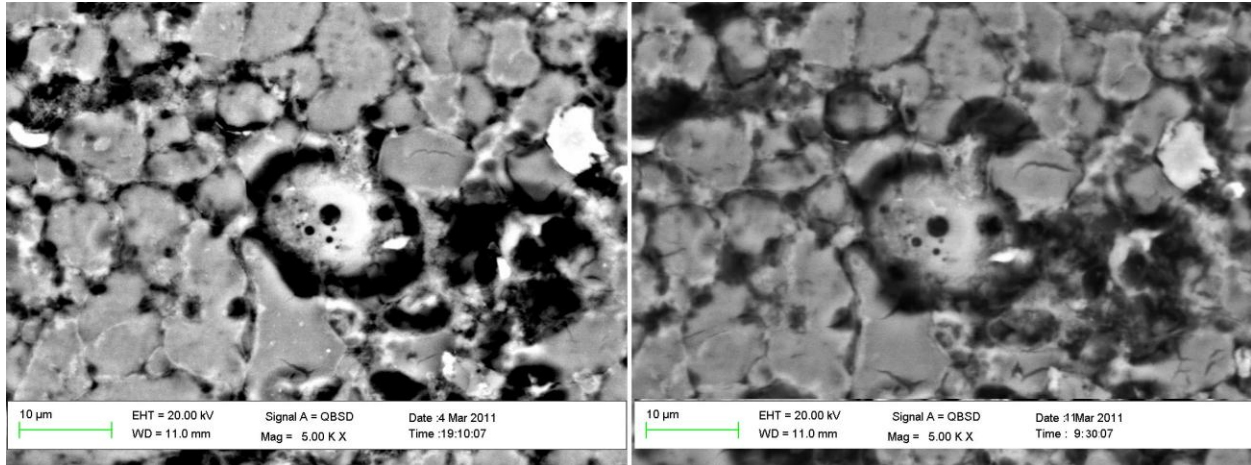


**Fig. 9: SEM micrographs the Fig. 7 zone 2 surface area after (a) 50h and b) 200h of immersion in the electrolyte**

The SEM micrographs and EDXS analyses of the representative area of the Al/20%KFA specimen confirmed the degradation mechanisms observed for the Al/10%KFA specimens. The degradation phenomena appear more intense for the Al/20%KFA specimens due to the higher amount of FA particles embedded into the metal matrix.

## CONCLUSIONS

In this work the electrochemical behaviour of Al matrix composites containing different amounts of a high calcareous ASTM Class C 618 FA has been studied.

Pure Al sintered specimens display the existence of Fe-rich intermetallics. These present cathodic behaviour relative to the Al matrix and act as preferential sites for pitting corrosion due to galvanic coupling leading to the breakdown of the Al passive layer.

The incorporation of the KFA particles leads to the formation of a heterogeneous microstructure. This is shown on SEM micrographs as well as on both topographic and Volta potential maps. FA particles with different sizes are randomly distributed into the Al matrix leading to the formation of areas with different Volta potential on the sample surface. Potentiodynamic polarization curves show a marked decrease of the corrosion potential and an increase of the corrosion current density associated to lower corrosion resistance in comparison to the pure Al specimens. This behaviour could be related to the effect of the FA particles, which impair the passive behaviour of the Al matrix.

The degradation phenomena occurring on the FA containing samples might be related to the following mechanisms: 1) Partial dissolution of the FA soluble phases, 2) dissolution of the Al matrix surrounding the FA particles due to crevice corrosion 3) Al localized dissolution due to galvanic coupling between the Fe-rich intermetallics and the matrix. Based on the degradation morphology it might be stated that the dissolution of the soluble FA phases and the crevice corrosion are the main degradation mechanisms. Finally it was observed that localized attack was more intense for the samples with the higher amount of FA.

## REFERENCES

- [1] Rohatgi, P. K., JOM,1994, 46, p. 55.
- [2] Daoud, A., Materials Science and Engineering A, 2009, 525, p. 7.
- [3] Karayiannis, V.G., Moutsatsou, A., Journal of Materials Processing Technology , 2006, 171, p. 295.
- [4] Hassan, S.F., Gupta, M., Materials Science and Engineering A, 2006, 425, p. 22.
- [5] Hajjari, E., Divandari, M., Materials and Design, 2008, 29, p. 1685.
- [6] Rajan, T.P.D., Pillai, R.M., Pai, B.C., Satyanarayana, K.G., Rohatgi, P.K., Composites Science and Technology, 2007, 67, p. 3369.
- [7] Daoud, A., Abou El-Khair, M.T., Shenouda, A.Y., Mohammed, E., Rohatgi, P.K., Materials Science and Engineering A, 2009, 526, p. 225.
- [8] Gupta, N., Gupta, K., Mueller, B.J., Materials Science and Engineering A, 2008, 485 p. 439.
- [9] Karayiannis, V.G., Moutsatsou, A., Journal of the European Ceramic Society, 2007, 27, p. 843.
- [10] Mondal, D.P., Das, S., Ramakrishnan, N., Uday Bhasker, K., Composites: Part A, 2009, 40, p. 279.
- [11] Rohatgi, P.K., Kim, J.K., Guo, R.K., Robertson, D.P., Gajdardziska-Josifovska, M., Metallurgical and Materials Transactions A, 2002, 33A, p. 1541.
- [12] Sudarshan Surappa, M.K., Material Science and Engineering A, 2008, 480, p. 117.
- [13] Moutsatsou, A., Itskos, G., Vounatsos, P., Koukouzas, N., Vasilatos, C., Material Science and Engineering A, 2010, 527, p. 4788.
- [14] Rohatgi, PK, Daoud, A, Schultz, BF, Puri, T., Composites: Part A ,2009, 40 (6-7), p.883.
- [15] Trowsdale, A.J., Noble, B., Harris, S.J., Gibbins, I.S.R., Thompson, G.E., Wood, G.C.. Corrosion Science, 1996, 38, p.177.
- [16] Coleman, S.L., Scott, V.D., McEnaney, B., Journal of Materials Science, 1994, 29, p.2826.
- [17] Pardo, A., Merino, M.C., Merino, S., Viejo, F., Carboneras, M., Arrabal, R., Corrosion Science, 2005, 47, p.1750.
- [18] Ahmad, Z., Paulette, P.T., Aleem, B.J.A., Journal of Materials Science, 2000, 35 p.2573.
- [19] Roper, G.W., Attwood, P.A., Journal of Materials Science, 1995, 30, p.898.
- [20] Birbilis, N., Buchheit, R.G., Journal of the Electrochemical Society, 2005, 152, p.B140.
- [21] Nisancioglu, K., Davanger, K.Y., Strandmyr, O., Journal of the Electrochemical Society, 1981, 128, p.1523.
- [22] Park, J.O., Paik, C.H., Huang, Y.H., Alkire, R.C., Journal of the Electrochemical Society, 1999, 146, p.517.
- [23] vom Berg, W., Lutze, D., "Handbook on fly ash in concrete", 2010, Verlag Bau+Technik GmbH.